PAPER • OPEN ACCESS

Recapitulating monocyte extravasation to the synovium in an organotypic microfluidic model of the articular joint

View the article online for updates and enhancements.

Biofabrication

Recapitulating monocyte extravasation to the synovium in an organotypic microfluidic model of the articular joint

Carlotta Mondadori[1,6] , Silvia Palombella[1,6] , Shima Salehi[1] , Giuseppe Talò[1] , Roberta Visone[2] , Marco Rasponi[2] , Alberto Redaelli[2] , Valerio Sansone[3] , Matteo Moretti[1,4,5] and Silvia Lopa[1,*]

1   IRCCS Istituto Ortopedico Galeazzi, Cell and Tissue Engineering Laboratory, 20161 Milan, Italy
2   Department of Electronics, Information and Bioengineering, Politecnico di Milano, 20133 Milan, Italy
3   IRCCS Istituto Ortopedico Galeazzi, 20161 Milan, Italy
4   Regenerative Medicine Technologies Lab, Ente Ospedaliero Cantonale, 6900 Lugano, Switzerland
5   Euler Institute, Faculty of Biomedical Sciences, Università della Svizzera Italiana, 6900 Lugano, Switzerland
6   Equally contributing authors.
*   Author to whom any correspondence should be addressed.

E-mail: silvia.lopa@grupposandonato.it

Abstract

The synovium of osteoarthritis (OA) patients can be characterized by an abnormal accumulation of macrophages originating from extravasated monocytes. Since targeting monocyte extravasation may represent a promising therapeutic strategy, our aim was to develop an organotypic microfluidic model recapitulating this process. Synovium and cartilage were modeled by hydrogel-embedded OA synovial fibroblasts and articular chondrocytes separated by a synovial fluid channel. The synovium compartment included a perfusable endothelialized channel dedicated to monocyte injection. Monocyte extravasation in response to chemokines and OA synovial fluid was quantified. The efficacy of chemokine receptor antagonists, RS-504393 (CCR2 antagonist) and Cenicriviroc (CCR2/CCR5 antagonist) in inhibiting extravasation was tested pre-incubating monocytes with the antagonists before injection. After designing and fabricating the chip, culture conditions were optimized to achieve an organotypic model including synovial fibroblasts, articular chondrocytes, and a continuous endothelial monolayer expressing intercellular adhesion molecule-1 and vascular cell adhesion molecule-1. A significantly higher number of monocytes extravasated in response to the chemokine mix ($p < 0.01$) and OA synovial fluid ($p < 0.01$), compared to a control condition. In both cases, endothelium pre-activation enhanced monocyte extravasation. The simultaneous blocking of CCR2 and CCR5 proved to be more effective ($p < 0.001$) in inhibiting monocyte extravasation in response to OA synovial fluid than blocking of CCR2 only ($p < 0.01$). The study of extravasation in the model provided direct evidence that OA synovial fluid induces monocytes to cross the endothelium and invade the synovial compartment. The model can be exploited either to test molecules antagonizing this process or to investigate the effect of extravasated monocytes on synovium and cartilage cells.

1. Introduction

Osteoarthritis (OA) is the most common type of arthritis and the fastest growing cause of disability worldwide [1, 2]. Although articular cartilage has long been considered the only relevant tissue in OA, a more recent approach defines OA as a whole-joint disease [3, 4], recognizing synovial inflammation as an active component of OA [5, 6]. OA synovium can in fact show pathological changes, such as an abnormal infiltration of macrophages [6, 7] that originate from circulating monocytes and sustain inflammatory processes [1, 8, 9]. Since disease-modifying OA drugs (DMOADs) still represent an unmet clinical need, recent evidences linking inflammation and OA pave the way to inflammation-targeting interventions

to hamper OA progression [1, 7, 10]. Targeting the excessive recruitment of monocytes to synovium may represent a suitable strategy to prevent the negative effects of macrophage accumulation, as proposed for other diseases [11]. To this aim, a deeper understanding of monocyte extravasation in the context of OA is crucial to identify specific chemokine-signaling axes involved in monocyte recruitment and test molecules antagonizing this event.

Extravasation is a multi-step process involving ordered interactions between circulating and endothelial cells [12]. Lately, 3D organotypic microfluidic models have found broad application to investigate this process [13, 14]. The advantages of microfluidic settings comprise the possibility to model tissues in compartmentalized 3D microenvironments including tissue-specific cells and perfusable endothelialized channels, control biophysical and biochemical stimulations, and monitor cell behavior in real-time. Finally, differently from Boyden or parallel plate flow chambers, the impact of gravity force on extravasation can be minimized. The vast majority of microfluidic extravasation models have been developed to investigate cancer cell and neutrophil behavior [13], while monocytes/macrophages have been applied in very few models related to cancer research [15, 16]. In fact, to the best of our knowledge, no microfluidic model has been designed to specifically study monocyte extravasation in the context of an articular disease, such as OA.

Our aim was to develop a model including primary human cells and pathological synovial fluid from OA patients to recapitulate the process of monocyte extravasation to the synovium. Specifically, we developed a 3D microfluidic organotypic model reproducing synovial compartments with a perfusable endothelialized channel, a channel for synovial fluid injection mimicking the articular cavity, and a cartilage compartment. Here, we describe the development of the model and its exploitation to investigate monocyte extravasation and the ability of OA synovial fluid to induce this process. Finally, we show how this model can be used to test molecules interfering with monocyte extravasation.

2. Materials and methods

2.1. Experimental set-up
To recapitulate the process of monocyte extravasation to the OA joint (figure 1(a)), we designed a microfluidic chip including synovial and chondral compartments, a channel dedicated to the endothelial monolayer formation, and a channel for synovial fluid injection (figure 1(b)). The first step of the experimental set-up is the injection of SFbs and articular chondrocytes (ACs) embedded in fibrin gel in their respective gel compartments. Once the gel is polymerized, the channel that separates the two synovial compartments is coated with fibronectin for 1 h and then endothelial cells are injected. The model is cultured for 24 h to allow the formation of a continuous endothelial monolayer, which is then subjected to 3 h of preconditioning with fluid flow and inflammatory stimulation. During this timeframe, monocytes are isolated to be injected in the endothelial channel as soon as the preconditioning phase is over. Simultaneously, synovial fluid is injected in the synovial fluid channel. After 18 h, monocyte extravasation is assessed by confocal microscopy.

2.2. Microfluidic chip design and fabrication
To satisfy our experimental needs, the final configuration of the microfluidic chip designed by CAD software (AutoCAD, AutoDesk Inc.) included three gel compartments and two microfluidic channels (figures 1(c) and (d)). Gel compartments were lined by regularly spaced trapezoidal posts and a 400 μm width was selected to minimize gel leakage during injection. The endothelial channel was sized starting from post-capillary venule dimensions (Ø: 20–50 μm) and balancing this *desideratum* with fabrication limits and ease-of-use, which resulted in a 200 μm wide channel. Considering synovial fluid viscosity, a 400 μm wide channel was designed to facilitate synovial fluid injection. The optical mask obtained using Adobe Illustrator CC (Adobe Systems Inc.) was printed on a polyester film and used to transfer the patterns on a SU-8 negative photoresist spin-coated on a silicon wafer to create the master mold. The microfluidic chips were then fabricated by polydimethylsiloxane replica molding by pouring silicone base and curing agent (10:1 mix) on molds and curing at 65 °C for 3 h. The fluidic ports were punched with different size. The inlets and outlets of the gel compartments (numbered 1 and 2 in figure 1(d)) were punched with 1 mm-diameter. The inlets of the endothelial and synovial fluid channels (numbered 3 and 5 in figure 1(d)) were also punched with 1 mm-diameter, while the outlets of the channels (numbered 4 and 6 in figure 1(d)), which also acted as medium/synovial fluid reservoirs, were punched with 4 mm-diameter. After punching the fluidic ports, chips were plasma bonded to glass slides (Harrick plasma).

2.3. Cell isolation and culture
Synovium, articular cartilage, and synovial fluid were obtained from OA patients undergoing knee replacement who signed an informed consent (inclusion criteria: 60–80 years, Kellgren-Lawrence ⩾III, presence of synovitis, non-steroidal anti-inflammatory drugs (NSAID) suspension at least one week before surgery). Synovium was digested with 3 mg ml^{-1} collagenase type I (Worthington Biochemical Corporation) at 37 °C for 2 h.
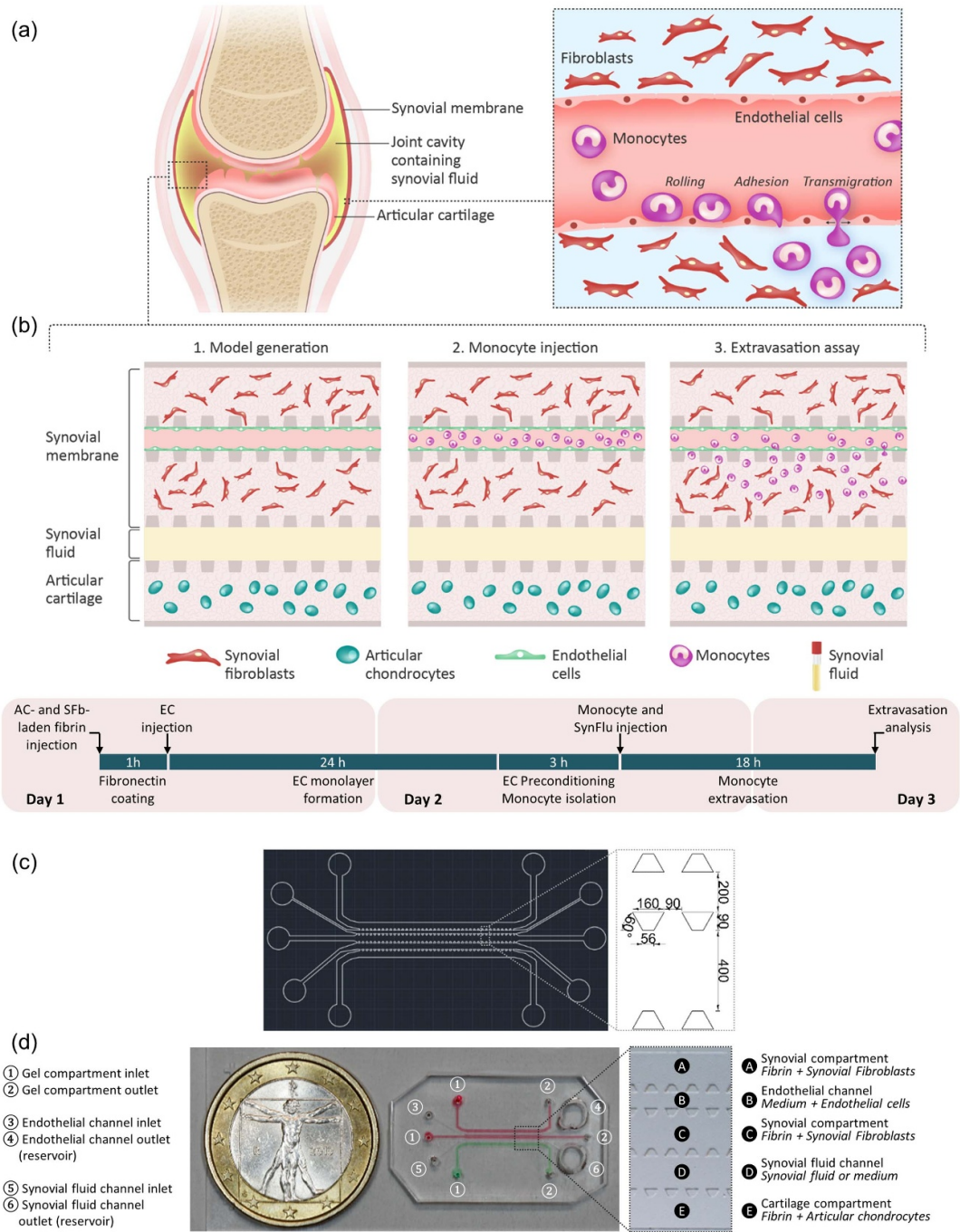
Figure 1. Development of a microfluidic organotypic model to study monocyte extravasation. (a) Illustration showing the articular joint and the process of monocyte extravasation responsible of increased monocyte infiltration in the OA synovium. (b) The experimental phases develop over a time course of 3 d and include: (1) the generation of the organotypic model, (2) the injection of monocytes in the endothelialized channel, and (3) the quantification of extravasated monocytes. (c) AutoCAD drawing of the microfluidic device. Trapezoidal posts are used to confine gel compartments. In evidence, the endothelial channel and the lower synovial compartment (respective width: 200 and 400 μm). (d) Top-view of the microfluidic device with the synovium (in red) and cartilage (in green) compartments in evidence. The inset shows a stereomicroscope image of the microfluidic chip features. The different elements of the chips are indicated by numbers and letters and identified in the lateral legends.

SFbs were plated (5×10^3 cells cm^{-2}) in complete medium (CM) composed of Dulbecco's modified Eagle medium (Gibco), 10% fetal bovine serum (FBS, Hyclone), 2 mM L-glutamine, 100 U ml^{-1} penicillin, 100 μg ml^{-1} streptomycin, 10 mM 4-(2-hydroxyethyl)-1-piperazineethanesulfonic acid

(HEPES), 1 mM sodium pyruvate (all from Gibco). Cartilage was digested with 1.5 mg ml^{-1} collagenase type II (Worthington Biochemical Corporation) at 37 °C for 18 h. ACs were plated (10×10^3 cells cm^{-2}) in CM supplemented with 0.4 mM L-proline and 50 μg ml^{-1} L-ascorbic

acid-2-phosphate (Sigma-Aldrich) [17]. Synovial fluid was centrifuged at 3000 *g* at 4 °C for 10 min and supernatant was stored at −80 °C. Primary green fluorescent protein-expressing human umbilical vein endothelial cells (GFP-HUVECs, Angio-Proteomie) at passage five were thawed and expanded in Endothelial cell growth medium-2 (EGM-2, Lonza) before use. Human primary monocytes were isolated from buffy coats of blood donors or whole blood of OA patients. After Ficoll (GE Healthcare) separation, monocytes were isolated by CD14 microbeads (Miltenyi Biotech) [18], stained with Vybrant™ Did (Molecular Probe) and suspended in Roswell Park Memorial Institute 1640 Medium (RPMI-1640, Gibco) with 2% FBS, 2 mM L-glutamine, 100 U ml^{-1} penicillin, 100 μg ml^{-1} streptomycin for extravasation experiments.

2.4. Optimization of culture conditions in fibrin gel
Different fibrin concentrations (5, 10, 20 mg ml^{-1}) and cell densities (2.5×10^6, 5×10^6 cells ml^{-1}) were tested. For fibrin embedding, cells were suspended in human thrombin (4 UI ml^{-1} in 40 mM CaCl$_2$, Baxter), mixed 1:1 with human fibrinogen (Sigma-Aldrich), and injected in the chip [19]. After gel polymerization (2–7 min, 37 °C), CM was injected into medium channels and chips were cultured for 48 h. Cell viability was assessed by Live/Dead assay (ThermoFisher Scientific). Images were acquired by fluorescence microscopy (Olympus IX-71, Olympus Corporation) and cells were counted by ImageJ.

2.5. Endothelial cell seeding
GFP-HUVECs were used for endothelial monolayer formation [20, 21]. After fibrin polymerization, the endothelial channel was incubated with 10 μg ml^{-1} human fibronectin (Millipore) for 1 h. Afterwards, endothelial cells suspended (6×10^6 cells ml^{-1}) in EGM-2 with 20% FBS were added to the endothelial channel outlet. The chip was maintained sloping for 10 min to facilitate cell entry using a customized 3D printed support (supplementary material S1 (available online at stacks.iop.org/BF/13/045001/mmedia)). After 20 min, EGM-2 and CM were added to the outlets of the endothelial and synovial fluid channels and chips were cultured for 24 h to allow monolayer formation.

2.6. Permeability and chemokine diffusion assay
To assess the endothelial monolayer integrity, a 70 kDa Fluorescein isothiocyanate (FITC)-dextran solution (800 μg ml^{-1}, Sigma-Aldrich) was injected in the endothelial channel and its diffusion towards the lower synovial compartment was monitored by fluorescence microscopy [22]. Chemokine diffusion was modeled injecting a 10 kDa FITC-dextran solution (800 μg ml^{-1}, Sigma-Aldrich),

approaching chemokine weight [23], in the synovial fluid channel and monitoring its diffusion over time. Chips without endothelial cells were used as control. Images were analyzed by ImageJ.

2.7. Computational modeling of wall shear stress
The shear stress along the endothelial wall was calculated by computational fluid dynamic (CFD) simulations (COMSOL Multiphysics 4.3b, AB), applying Navier–Stokes equations for an incompressible flow (ρ: density; u: velocity; t: time; μ: dynamic viscosity; p: pressure; F: external forces applied to the fluid):

$$\rho \left(\frac{\partial u}{\partial t} + u \nabla u \right) = \nabla \left[-pI + \mu \left(\nabla u + (\nabla u)^{\mathrm{T}} \right) \right] + F. \tag{1}$$

The continuity equation yields:

$$\rho \nabla u = 0. \tag{2}$$

The endothelial channel was modeled as a rectangular domain with a numerical grid containing 2165 240 tetrahedral elements. Modeling the endothelial channel with a rectangular domain implied an approximation that neglected possible gel deformations in correspondence of the gaps between adjacent pillars. However, since gel deformations depend mainly on fibrin shrinkage and are hardly predictable, modeling the channel with a rectangular domain represented the most reliable way to get an indication about the range of shear stress levels applied on endothelial cells in the different flow conditions. Culture medium was modeled with $\rho = 1000$ kg m^{-3} and $\mu = 0.00082$ Pa × s [24]. Boundary conditions were: (a) $p = 0$ Pa and $u = 0$ m s^{-1} in the domain before starting the simulation; (b) laminar inflow equal to 5, 10, 15, and 30 μl h^{-1} at the inlet; (c) $p = 0$ Pa at the outlet.

2.8. Effect of flow and Tumor Necrosis Factor-α (TNF-α) on endothelial cells
Twenty-four hours after injection, endothelial cells were perfused at 5, 10, 15, or 30 μl h^{-1} by syringe pump (Harvard Apparatus PHD 2000) or maintained in static conditions for 3 h, using EGM-2 added or not with 10 ng ml^{-1} TNF-α (PeproTech). For immunostaining, samples were fixed with 2% paraformaldehyde for 10 min, incubated with 1% bovine serum albumin (Sigma-Aldrich) in Hanks' balanced salt solution (HBSS, Gibco) for 30 min at r.t., and subsequently incubated at 4 °C o.n. with primary antibodies. Intercellular adhesion molecule 1 (ICAM-1) and vascular cell adhesion molecule-1 (VCAM-1) were detected using a mouse monoclonal antibody (sc-18853, 1:100, SantaCruz Biotechnology) and a rabbit monoclonal antibody (ab134047,

1:200, Abcam), respectively. After washing, samples were incubated 1 h at 37 °C with secondary antibodies: goat anti-mouse AlexaFluor-647 (A21235, 1:1000, ThermoFisher Scientific) and goat anti-rabbit AlexaFluor-647 (A21244, 1:500, ThermoFisher Scientific). Nuclei were stained with 2.5 μM Syto82 (ThermoFisher Scientific) for 2 min at r.t. Images were acquired by confocal microscopy (Leica SP8).

2.9. Monocyte extravasation in response to chemokines

To validate the model, monocyte extravasation in response to a chemokine mix was quantified. After preparing the organotypic culture, chips were either perfused for 3 h at 30 μl h^{-1} in the presence of 10 ng ml^{-1} TNF-α or maintained in static conditions without TNF-α. To assess the integrity of the endothelial monolayer after preconditioning with flow and TNF-α, a suspension of red polystyrene microbeads (1:5 dilution in EGM-2) characterized by a diameter resembling that of human monocytes (Ø 10 μm) was injected in the endothelial channel using the same protocol applied for monocyte injection to verify if the microbeads could invade the surrounding gel compartments due to the presence of holes in the monolayer. Human primary monocytes from five buffy coats were used in subsequent extravasation experiments. After isolation and staining, monocytes were suspended in RPMI-1640 medium (4×10^6 cells ml^{-1}) and added to the endothelial channel outlet. The device was maintained sloping for 15 min to facilitate monocyte entry. CM containing 2% FBS, 50 ng ml^{-1} CCL2, 50 ng ml^{-1} CCL3, 50 ng ml^{-1} CCL4, 50 ng ml^{-1} CCL5 was injected in the synovial fluid channel to induce monocyte extravasation. CM without chemokines was used in control chips. After 18 h, pictures were taken by confocal microscope acquiring the entire channel height and analyzed by ImageJ to quantify extravasated monocytes in two ROI representing the two synovial compartments. Images were processed by Imaris (Bitplane Software) to allow a better visualization of extravasated monocytes in the figures.

2.10. Monocyte extravasation in response to OA synovial fluid

Monocyte extravasation in response to OA synovial fluid was investigated. Microfluidic chips were prepared by injecting the compartments with plain or cell-loaded gels. Before fibrin embedding, SFbs and ACs were respectively stained with Vybrant™ DiI and DiO (Molecular Probe). Endothelial cells were seeded in the endothelial channel and cultured for 24 h to allow monolayer formation. Chips were perfused for 3 h at 30 μl h^{-1} in the presence of 10 ng ml^{-1} TNF-α or maintained in static conditions without TNF-α. Primary human monocytes isolated from seven buffy coats were used in extravasation experiments. A mix of synovial fluids obtained from three

OA patients was injected in the synovial fluid channel. CM with 2% FBS was used as control. After 18 h, a z-stack corresponding to the entire channel height was acquired by confocal microscopy and monocyte extravasation was quantified. To monitor extravasation in time lapse, monocytes were injected in preconditioned endothelial channels, and chips were maintained o.n. in an environmental chamber, taking pictures every 10 min.

2.11. Screening of chemokine receptor antagonists

RS-504393, a single antagonist for CCR2, and Cenicriviroc (CVC), a CCR2/CCR5 dual antagonist, were purchased from Tocris and Axon MedChem. Primary human monocytes were isolated from whole blood of five OA patients and stained with Vybrant™ Did. Monocytes were incubated 3 h at 37 °C in RPMI-1640 medium added with vehicle (Dimethyl sulfoxide, DMSO) or antagonist (RS-504393 or CVC, 1 μM). Unbound inhibitor was washed before adding monocytes to the endothelial channel inlet. All the chips injected with monocytes pre-incubated with RS-504393 or CVC contained a mix of synovial fluid pooled from three OA patients. Monocytes pre-incubated with vehicle were injected in chips containing either synovial fluid (positive control) or control medium (negative control). After 18 h, images were acquired by confocal microscopy and monocyte extravasation quantified.

2.12. Statistical analysis

For cell viability and FITC-dextran diffusion experiments, data were obtained from three samples per condition. In cell viability experiments, Two-Way ANOVA was applied to evaluate the combined effect of fibrin density and cell concentration. In FITC-dextran diffusion experiments, differences between control and endothelialized chips over time were tested by means of Two-Way ANOVA for repeated measures.

Independent extravasation experiments were performed using monocytes isolated from the buffy coats of five donors in the case of chemokine experiments, monocytes isolated from the buffy coats of seven donors for synovial fluid experiments, and from whole blood of five OA patients for the screening of CCR antagonists. In each experiment, two chips were prepared for each experimental condition. For each buffy coat or blood donor, a single value relative to the number of cells extravasated toward the upper or lower synovial compartment was obtained for each experimental condition by averaging the data obtained from multiple regions of the same chip and then by averaging the data obtained from multiple chips representing the same experimental conditions. In summary, five independent values for each experimental condition (one for each buffy coat/blood donor) were used in the statistical analysis

for chemokine-induced extravasation and CCR antagonist screening and seven independent values for each experimental condition (one for each buffy coat donor) were used in the statistical analysis for monocyte extravasation in response to synovial fluid. Differences within a single experimental group between the number of monocytes extravasated in the upper and lower compartment of the same chip were analyzed by means of Student's *t*-test for paired data. The combined influence of multiple variables on the number of extravasated monocytes was analyzed by Two-Way ANOVA. Bonferroni's post-hoc test was applied after Two-Way ANOVA. In the antagonist screening, the number of extravasated monocytes in the lower compartment was compared among groups by means of One-Way ANOVA for matched data, matching the data of each monocyte donor. All analyses were performed using GraphPad Prism (GraphPad Software).

3. Results

3.1. Optimization of culture conditions
The culture conditions for SFbs and ACs were optimized by assessing cell viability for different fibrin concentrations and cell densities (figure 2(a)). In all conditions, live cells clearly prevailed over dead cells, with about 80% of live cells detected after 48 h (figure 2(b)). No significant differences in terms of cell viability were found comparing different fibrin concentrations. In some experimental groups, a significantly higher cell viability was observed when the lowest cell density was used. Based on these results, we selected the lowest cell density (2.5×10^6 cells ml^{-1}) and the intermediate fibrin gel concentration (10 mg ml^{-1}) for subsequent experiments.

3.2. Assessment of endothelial monolayer integrity
In 24 h, a continuous endothelial monolayer formed with endothelial cells covering all channel sides (figure 2(c)). A permeability assay was performed by injecting a fluorescent tracer in the endothelial channel. Additionally, chemokine diffusion was simulated to verify that chemokines could reach the abluminal surface without diffusing in the endothelial channel. The permeability assay showed that in control chips (i.e. without endothelial cells) FITC-dextran was free to diffuse, reaching the synovial compartment soon after the injection. Conversely, the diffusion of FITC-dextran was significantly hindered by the endothelial barrier (figure 2(d)). Coherently, the FITC-dextran injected in the synovial fluid channel was free to diffuse in control chips, while the endothelial monolayer hampered its diffusion in the endothelial channel and induced its accumulation in the lower synovial compartment (figure 2(e)).

3.3. Endothelial monolayer preconditioning
To mimic the *in vivo* situation, the endothelial monolayer was preconditioned by biophysical and biochemical stimulation. Computational simulations showed that wall shear stress increased with increasing flow rates (figure 3(a)), with maximum shear stress estimated to be equal to 0.04, 0.07, 0.11, and 0.22 dyne cm^{-2} for flow rates of 5, 10, 15, and 30 μl h^{-1}, respectively. It should be underlined that these CFD simulations provided only an estimate of the shear stress levels applied on endothelial cells. In fact, modeling the endothelial channel with a rectangular domain implied an approximation that neglected any possible gel deformation in correspondence of the gaps between adjacent pillars. However, since gel deformations depended mainly on fibrin shrinkage and were hardly predictable, modeling the channel with a rectangular domain represented the most viable approach to get an indication about shear stress levels applied in the channel in the different flow conditions.

Perfusing the endothelial monolayer with flow rates up to 30 μl h^{-1} did not interfere with its integrity (figure 3(b)), whereas higher flow rates induced endothelial cell detachment (data not shown). The effect of shear stress on the expression of ICAM-1 and VCAM-1, two molecules mediating monocyte-endothelium adhesion, was then investigated. ICAM-1 was not expressed in static condition, while it was highly upregulated when samples were exposed to flow rates equal or higher than 10 μl h^{-1}. Differently, VCAM-1 was more expressed in static conditions and at low flow rates (figure 3(c), second row).

To mimic an inflammatory state, endothelial cells were exposed to TNF-α alone or combined with flow at 30 μl h^{-1}. ICAM-1 and VCAM-1 expression increased in the presence of TNF-α, both in static and dynamic conditions. Specifically, ICAM-1 was strongly upregulated in static samples treated with TNF-α and a synergic effect of flow and TNF-α was observed. Interestingly, ICAM-1 was expressed also by SFbs, especially in response to TNF-α (figure 3(d), first row). VCAM-1 expression was also upregulated by TNF-α, in both static and dynamic samples (figure 3(d), second row). Based on these results, monocyte extravasation assays were performed applying a preconditioning with flow at 30 μl h^{-1} and TNF-α.

3.4. Monocyte extravasation in response to chemokines
In extravasation experiments, the number of monocytes extravasated in chips with endothelial cells preconditioned or not by flow and TNF-α was compared to assess the effect of endothelial preconditioning on extravasation. To characterize the effect of endothelial preconditioning, the permeability of the endothelial monolayer was also evaluated
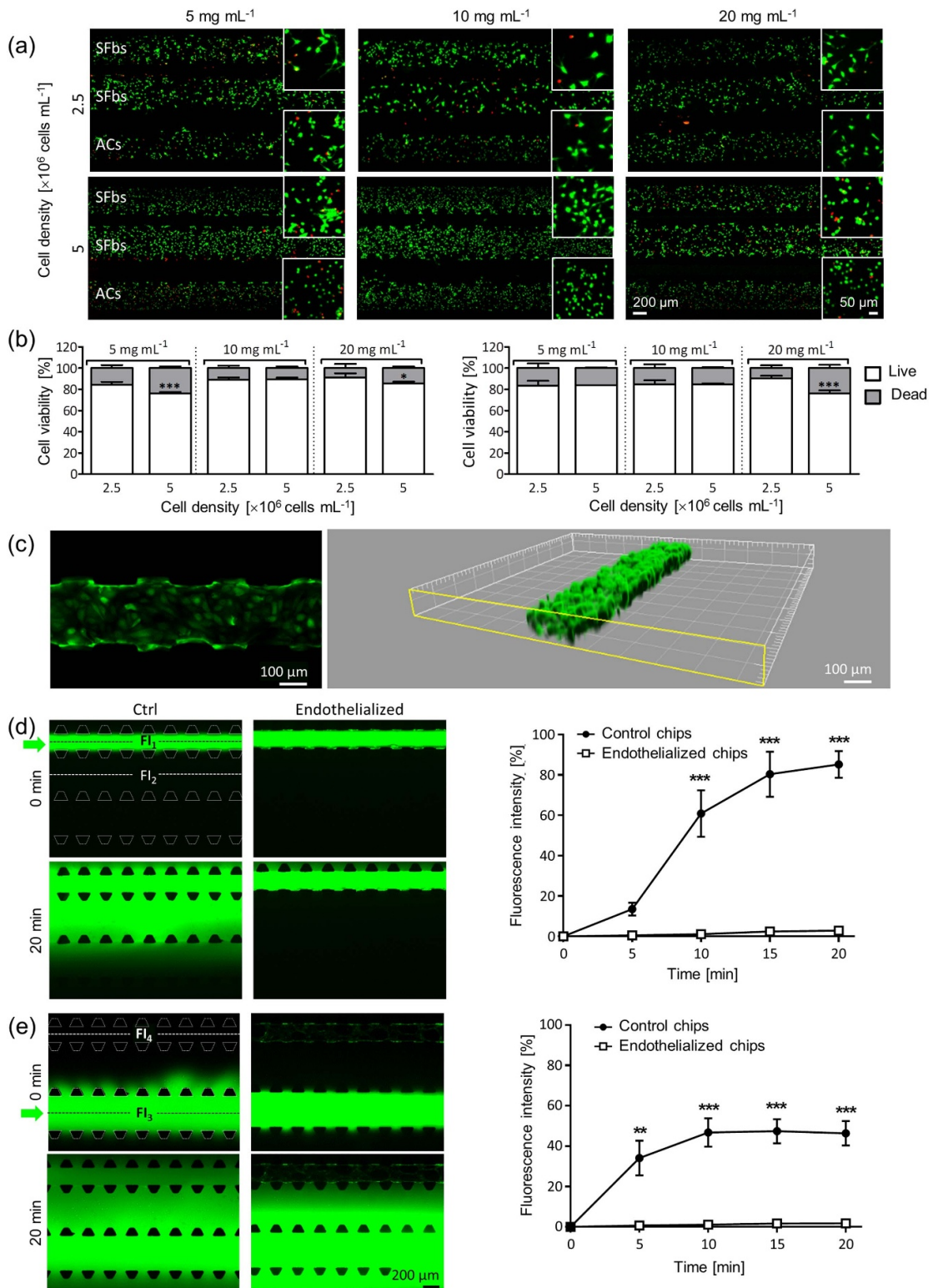
Figure 2. Cell culture in the microfluidic model. (a) Live/Dead of SFbs and ACs (2.5×10^6, 5×10^6 cells ml^{-1}) in different fibrin concentrations (5, 10, 20 mg ml^{-1}). (b) Viability of SFbs (left graph) and ACs (right graph) expressed as percentage of live and dead cells in the different conditions (mean + SE; 2.5×10^6 cells ml^{-1} vs 5×10^6 cells ml^{-1}: $***p < 0.001$; $*p < 0.05$). (c) Images showing the formation of a continuous endothelial monolayer in the channel. (d) Permeability assay and quantification of fluorescence intensity (FI) detected in center of the lower synovial compartment (FI2), normalized to the FI detected in the center of the endothelial channel (FI1). (e) Analysis of chemokine diffusion and quantification of FI detected in the center of the endothelial channel (FI4) normalized to the FI detected in the center of the synovial fluid channel (FI3) (mean ± SE; control vs endothelialized chips: $***p < 0.001$; $**p < 0.01$).
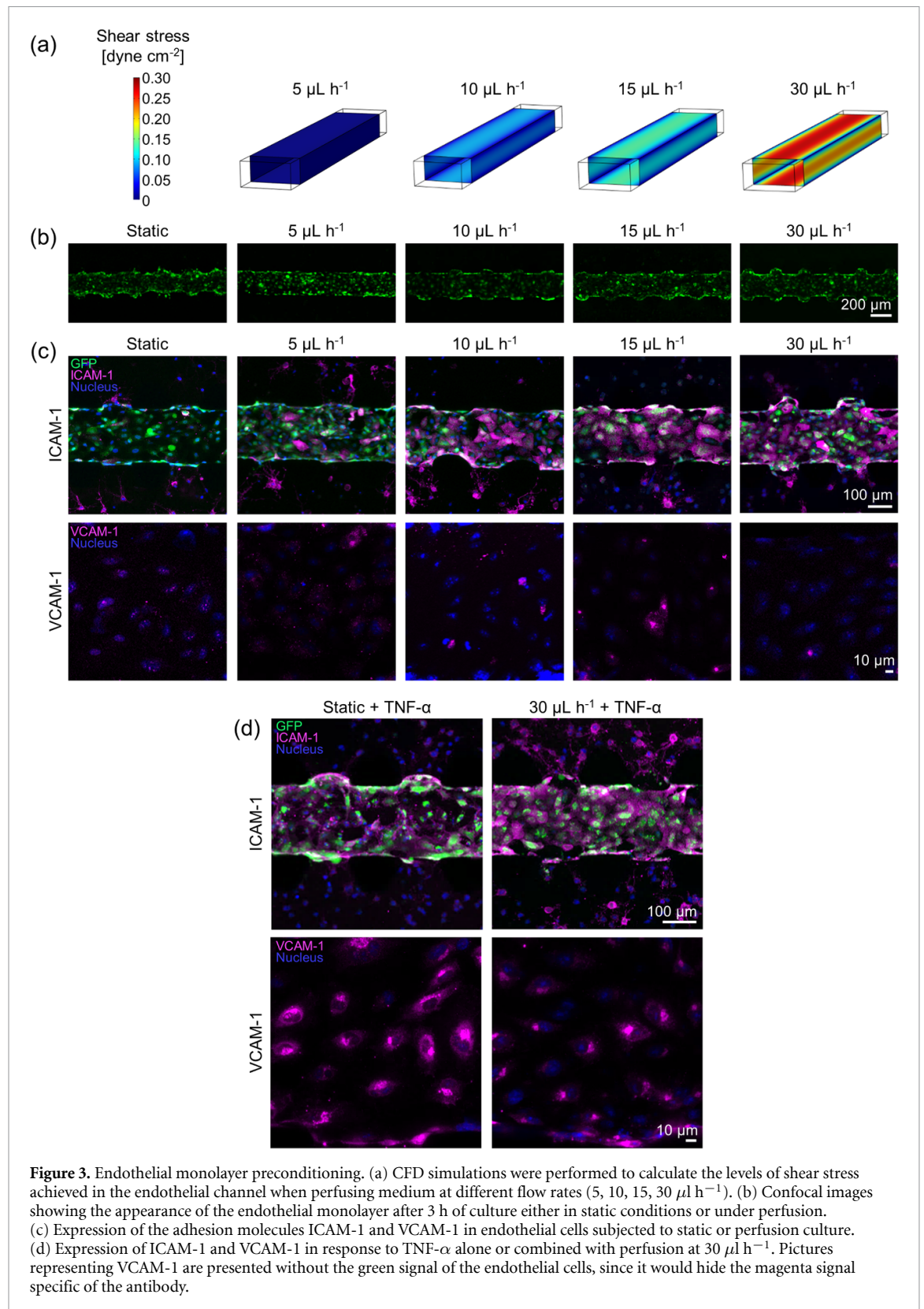
Figure 3. Endothelial monolayer preconditioning. (a) CFD simulations were performed to calculate the levels of shear stress achieved in the endothelial channel when perfusing medium at different flow rates (5, 10, 15, 30 μl h^{-1}). (b) Confocal images showing the appearance of the endothelial monolayer after 3 h of culture either in static conditions or under perfusion. (c) Expression of the adhesion molecules ICAM-1 and VCAM-1 in endothelial cells subjected to static or perfusion culture. (d) Expression of ICAM-1 and VCAM-1 in response to TNF-α alone or combined with perfusion at 30 μl h^{-1}. Pictures representing VCAM-1 are presented without the green signal of the endothelial cells, since it would hide the magenta signal specific of the antibody.

(figure 4(a)). The endothelium preconditioned with flow at 30 μl h^{-1} and TNF-α was characterized by a slight increase in endothelial permeability compared to the endothelium cultured in static conditions, but it maintained the ability to significantly hamper the diffusion of FITC-dextran from the endothelial channel compared to chips without

endothelium (***$p < 0.001$; figure 4(a)). Experiments conducted injecting microbeads with size comparable to that of human monocytes showed that the endothelial preconditioning did not generate gaps in the monolayer through which monocytes could enter the surrounding gel, which would bias the results of the extravasation assay (figure 4(b)). In

fact, independently from endothelial preconditioning, microbeads injected in the endothelial channel remained confined in the luminal side, as also shown by the videos (supplementary materials S2 and S3) where many microbeads rolling along the endothelial walls without entering the gel can be observed.

To validate the model, monocyte extravasation in response to a chemokine mix was quantified (figure 4(c)). Samples without the chemokine mix were used as control. Monocytes extravasated only in the presence of chemokines preferentially migrating into the lower synovial compartment, toward the chemokine mix, than to the upper compartment ($^{#}p < 0.05$; figure 4(c)), while they remained mostly confined in the endothelial channel when chemokines were not added (figure 4(b)). Endothelial preconditioning significantly promoted monocyte extravasation. In fact, the difference between the number of monocytes extravasated toward the lower compartment in chemokine and control samples was significant only when endothelial cells were preconditioned ($^{**}p < 0.01$; figure 4(c)).

3.5. Monocyte extravasation in response to OA synovial fluid

Monocyte extravasation in response to OA synovial fluid was determined in different conditions, including presence/absence of endothelial preconditioning and presence/absence of tissue-specific cells (figure 5(a)). A higher number of extravasated monocytes was measured in the lower synovial compartment in synovial fluid compared to control samples, with significant differences in favor of the synovial fluid group in almost all conditions ($^{*}p < 0.05$, $^{**}p < 0.01$; figure 5(b)). Consistently, time-lapse videos (supplementary materials S4 and S5) showed that monocytes extravasated toward the lower compartment only in the presence of synovial fluid, while they remained confined in the endothelial channel in control samples. Remarkably, albeit some monocytes extravasated also toward the upper compartment, the number of extravasated monocytes in the lower compartment was significantly higher in all the synovial fluid groups ($^{#}p < 0.05$, $^{##}p < 0.01$; figure 5(b)).

3.6. Screening of chemokine receptor antagonists

Chemokine receptors antagonists binding either CCR2 only or both CCR2 and CCR5 were tested in the model to assess their ability to inhibit the extravasation of monocytes isolated from OA patients in response to OA synovial fluid (figure 6(a)). The results of these experiments confirmed that monocyte extravasation was induced by OA synovial fluid as demonstrated by the higher number of extravasated monocytes detected in the synovial fluid group compared to controls ($^{***}p < 0.001$, figure 6(b)).

The extravasation of monocytes that had been pre-incubated with either RS-504393 or CVC in response to OA synovial fluid was significantly reduced compared to monocytes that had been pre-incubated with the vehicle before injection ($^{**}p < 0.01$; $^{***}p < 0.001$). In particular, the treatment of monocytes with CVC, which antagonizes both CCR2 and CCR5, yielded the most significant reduction with levels of extravasation like those detected in control samples, where the synovial fluid was not present.

4. Discussion

The unmet clinical need for DMOADs prompts the study of inflammation-related events to identify new potential therapy targets for OA. Here, we developed a microfluidic organotypic model comprising vascularized synovial and cartilage compartments to study the extravasation of monocytes, from which infiltrating macrophages originate. In the design phase, we sought for a balance between trying to match the *in vivo* complexity and the possibility to obtain reproducible results and manage multiple samples [25, 26]. Since our final goal was to develop a model for testing anti-chemokine drugs and, in the future, investigating the effect of infiltrating monocytes/macrophages on cartilage and synovium cells, we modeled only these tissues, whose cells are involved in a vicious cycle that propagates inflammation [1, 7].

Once fabricated the chip, we cultured ACs and SFbs in fibrin gel to provide cells with a natural biocompatible matrix [19, 27]. Fibrin finds wide application for 3D cell culture in microfluidic devices [13, 28]. In the perspective of extravasation models, where the endothelial compartment plays a key role, fibrin provides a physiological substrate conductive to endothelial assembly, as demonstrated in many *in vitro* models [29]. Additionally, fibrin matrix combines structural properties that remind those of collagenous matrix with ease-of-use since polymerization requires an activation step via thrombin cleavage and, hence, can be finely controlled and tuned [30–32]. Although the relevance of fibrin for synovial fibroblast and articular chondrocyte culture may be limited from a biological point of view, it should be considered that any mono-component matrix would fail in mimicking the compositional and structural complexity of native tissues. However, the intrinsic tendency of fibrin to be gradually degraded and replaced by extracellular matrix produced from fibrin-embedded cells [33, 34] combined with its structural properties and technical advantages make fibrin a good choice to establish microfluidic organotypic models.

After selecting the cell and fibrin concentration to be used in the model, we optimized the protocol to
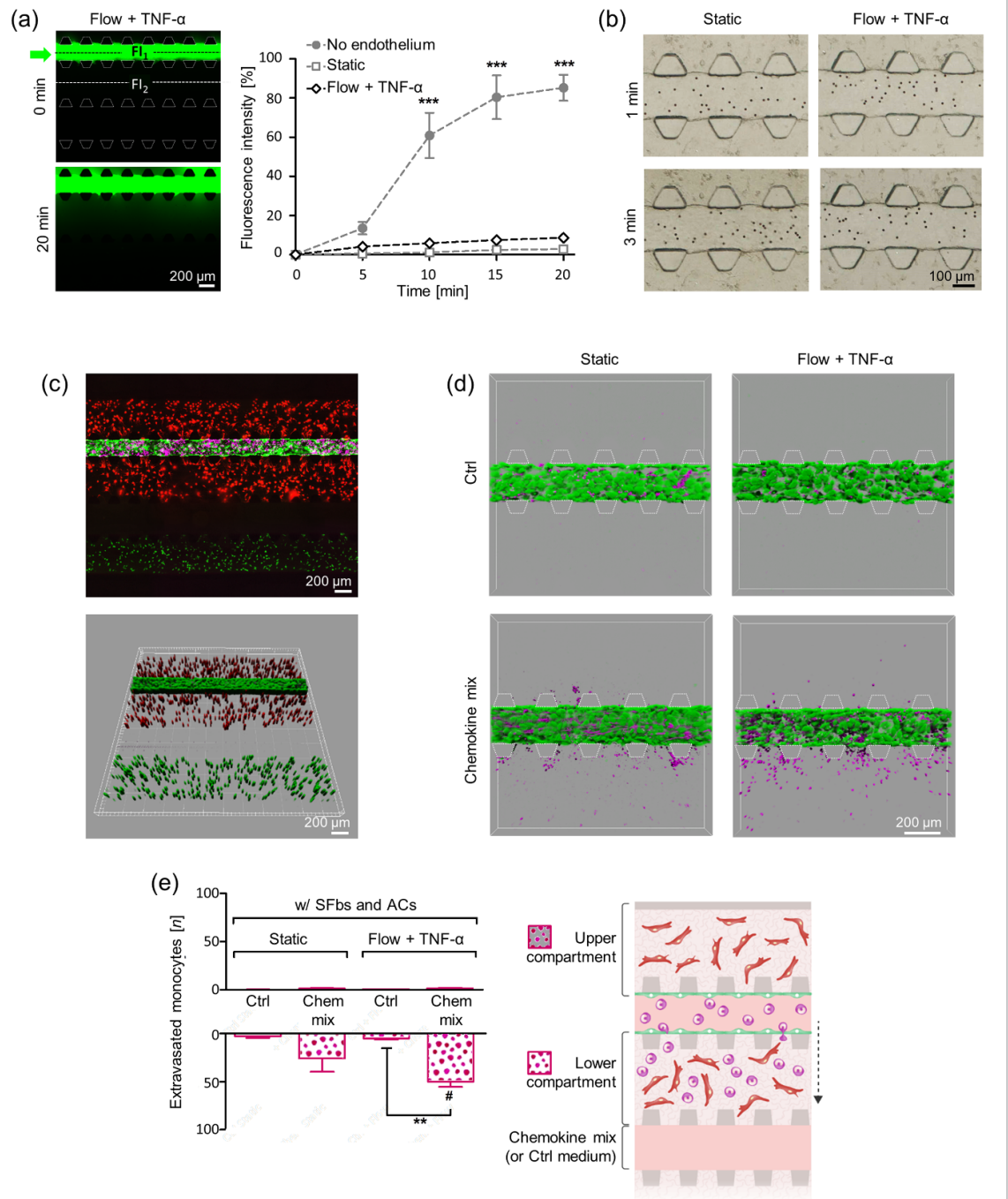
Figure 4. Monocyte extravasation in response to chemokines. (a) Permeability assay and quantification of the fluorescence intensity (FI) in center of the lower synovial compartment (FI2), normalized to the FI in the center of the endothelial channel (FI1) performed after endothelial preconditioning (flow at 30 μl h^{-1} + TNF-α). The data relative to FITC-dextran diffusion in chips without endothelium or with non-preconditioned endothelial cells presented in figure 2(d) are shown in the graph as comparison groups (mean $\pm$ SE; no endothelium vs flow + TNF-α: ***$p < 0.001$). (b) Pictures showing 10 μm microbeads confined in the endothelial channel at different time points after injection. (c) Pictures showing all the cell types (labeled with different cell trackers) in the model. The 3D reconstruction clarifies that immediately after injection monocytes are inside the endothelialized channel. From the top to the bottom: synovial fibroblasts in red, endothelial cells in green, monocytes in magenta, and articular chondrocytes in green. (d) Monocyte extravasation in response to a chemokine mix evaluated in static conditions or after endothelial preconditioning (flow at 30 μl h^{-1} + TNF-α) compared to control samples without chemokines (Ctrl). (e) Quantification of monocytes extravasated to the lower synovial compartment towards the chemokine stimulus compared to monocytes extravasated to the upper synovial compartment in all the tested conditions (mean + SE; lower compartment vs upper compartment: #$p < 0.05$. Control vs chemokine mix: **$p < 0.01$). The illustration shows the position of the compartments indicated as 'upper compartment' and 'lower compartment' in the graph.

achieve a perfusable endothelialized channel, characterized by a continuous monolayer. Monolayer continuity ensures that monocytes must actively contribute to cell junction remodeling to extravasate [12], in combination with the effect of a mediator such as TNF-α [35] that was applied in extravasation experiments to mimic an inflamed condition. Furthermore, a continuous monolayer allows creating different
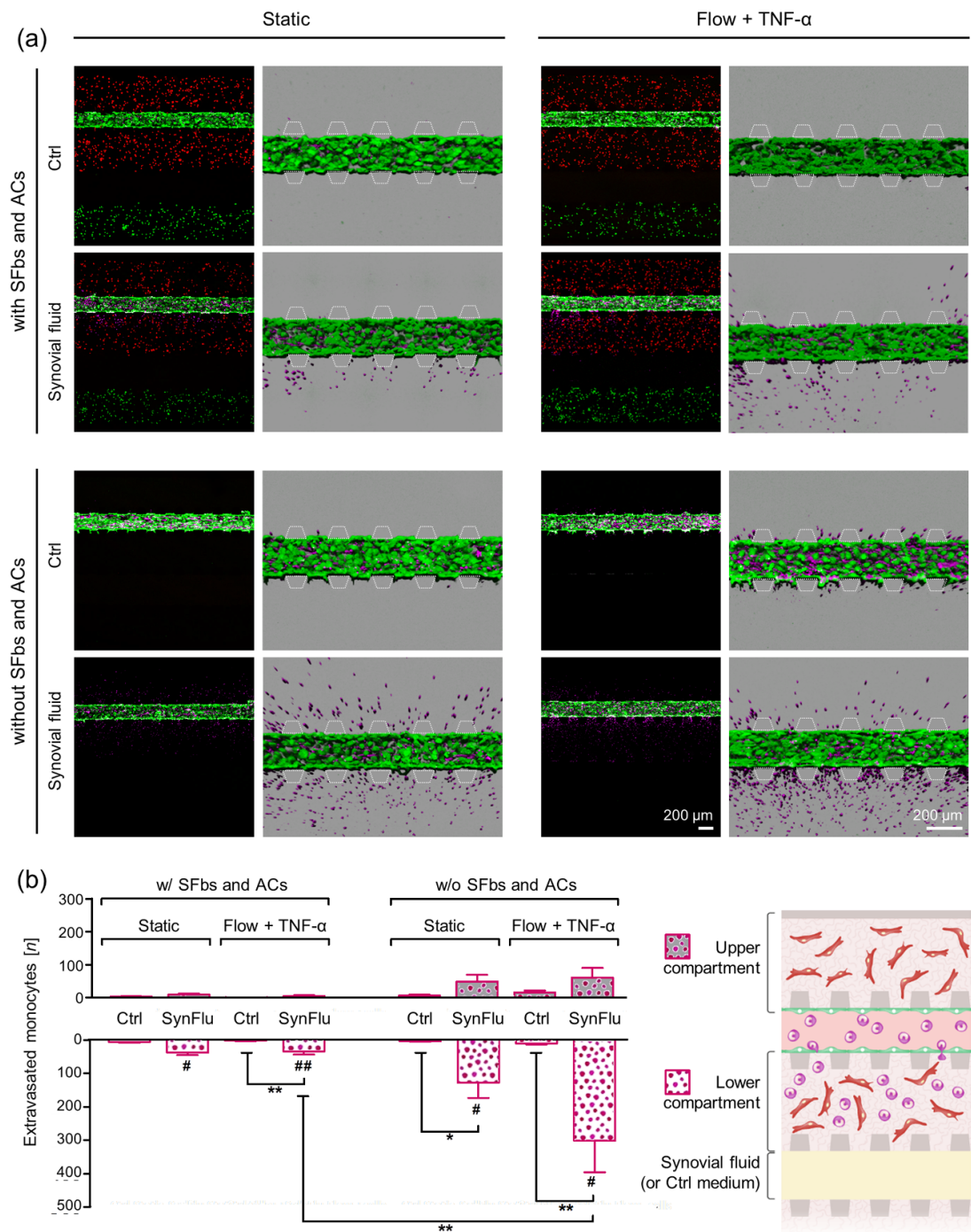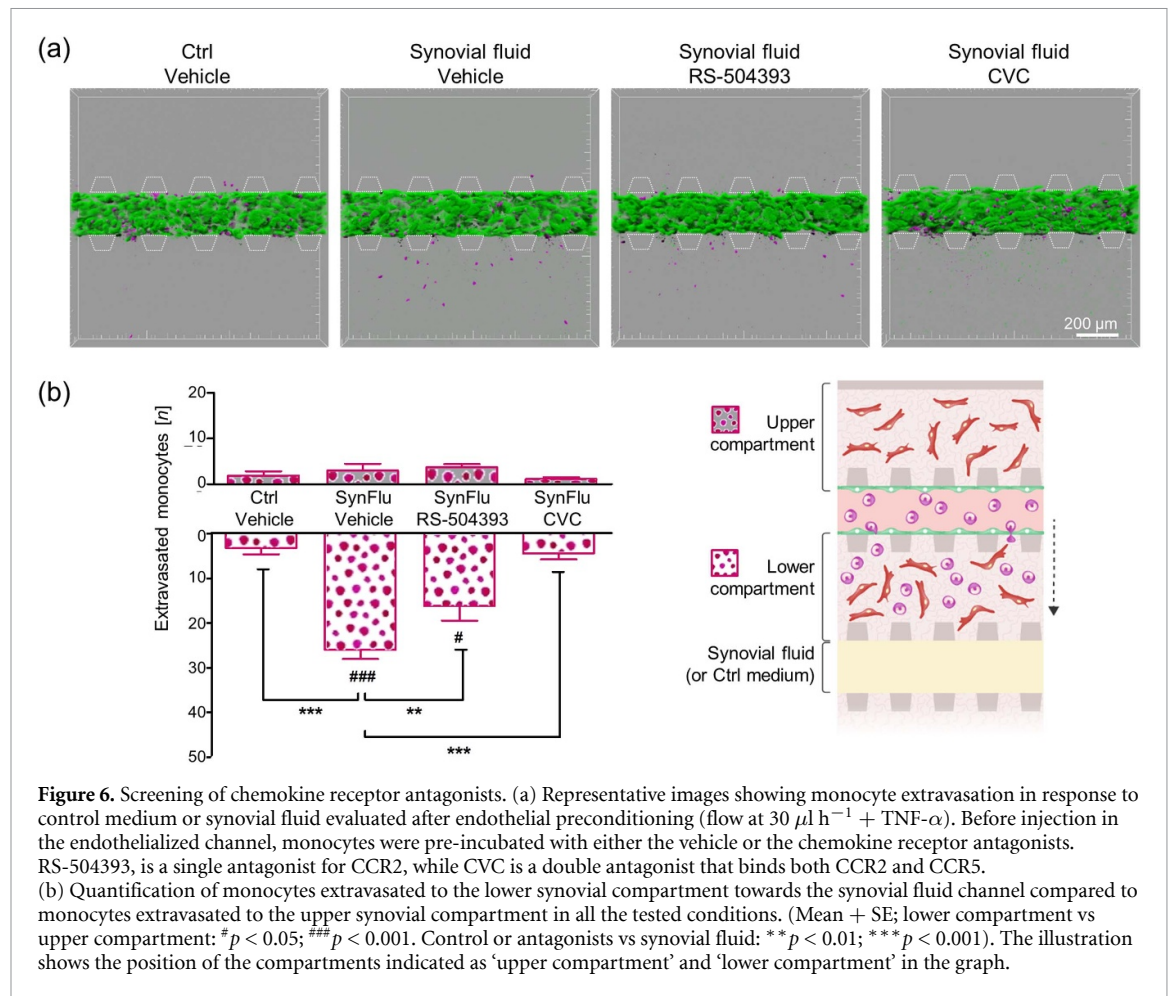
Figure 5. Monocyte extravasation in response to OA synovial fluid. (a) Monocyte extravasation in response to synovial fluid evaluated in static condition or after endothelial preconditioning (flow at $30 \, \mu l \, h^{-1}$ + TNF-α) compared to control samples. Extravasation was tested in the presence or in the absence of SFbs and ACs to assess the influence of tissue-specific cells on monocyte extravasation. (b) Quantification of monocytes extravasated to the lower synovial compartment towards the synovial fluid channel compared to monocytes extravasated to the upper synovial compartment in all tested conditions. (Mean + SE; lower compartment vs upper compartment: $^{\#}p < 0.05$; $^{\#\#}p < 0.01$. Control vs synovial fluid: $^{*}p < 0.05$; $^{**}p < 0.01$). The illustration shows the position of the compartments indicated as 'upper compartment' and 'lower compartment' in the graph.

microenvironments in the abluminal and luminal endothelium side, with a higher chemokine concentration maintained in the abluminal side over the entire experimental time course (supplementary material S6). This feature resembles the *in vivo* situation where chemokines produced by extravascular cells reach the abluminal side and are presented

by endothelial cells to circulating leukocytes in the luminal side [36]. However, leukocyte extravasation does not depend only on chemoattractants, but also on endothelial cell phenotype. The shear stress exerted by fluid flow can directly modulate molecules mediating the adhesion of circulating cells to the endothelium during extravasation [37]. Although the

Figure 6. Screening of chemokine receptor antagonists. (a) Representative images showing monocyte extravasation in response to control medium or synovial fluid evaluated after endothelial preconditioning (flow at 30 μl h^{-1} + TNF-α). Before injection in the endothelialized channel, monocytes were pre-incubated with either the vehicle or the chemokine receptor antagonists. RS-504393, is a single antagonist for CCR2, while CVC is a double antagonist that binds both CCR2 and CCR5.
(b) Quantification of monocytes extravasated to the lower synovial compartment towards the synovial fluid channel compared to monocytes extravasated to the upper synovial compartment in all the tested conditions. (Mean + SE; lower compartment vs upper compartment: $^{\#}p < 0.05$; $^{\#\#\#}p < 0.001$. Control or antagonists vs synovial fluid: $^{**}p < 0.01$; $^{***}p < 0.001$). The illustration shows the position of the compartments indicated as 'upper compartment' and 'lower compartment' in the graph.

applied shear stress levels were lower than physiological values (1–5 dyne cm^{-2}) [38], our experiments demonstrated that they affected endothelial cell phenotype. The expression of ICAM-1, almost absent in static conditions, increased for increasing flow rates, as shear stress levels were getting closer to physiological values, in line with studies showing that laminar flow upregulates ICAM-1 in endothelial cells [39] and subsequently promotes leukocyte adhesion [40]. On the other hand, VCAM-1 was more expressed in static conditions and at low flow rates than in response to higher shear stress levels, in agreement with data showing VCAM-1 downregulation by shear stress [41] and suggesting that VCAM-1 may mediate leukocyte adhesion low shear stress regions. Shear stress was combined with TNF-α to resemble an inflamed condition. TNF-α was selected as it activates inflammatory pathways in endothelial cells via NF-kB and is present at high levels in OA joints [1, 3]. Accordingly to data showing the synergic effect of shear stress and TNF-α on ICAM-1 and the opposite effect of these factors on VCAM-1 [42], in our experiments ICAM-1 and VCAM-1 expression was enhanced by TNF-α, with TNF-α partially rescuing the negative effect of shear stress on VCAM-1. Interestingly, TNF-α increased ICAM-1 expression also in SFbs, in line

with literature showing a dose-dependent effect of TNF-α on ICAM-1 in this cell type [43].

To test the reliability of the model, as usually done in standard migration assays [44], we compared the extravasation of monocytes in response to a chemokine mix with a control group. Chemokines (CCL2, CCL3, CCL4, and CCL5) with known chemotactic effect on monocytes were selected [44, 45]. Remarkably, monocyte extravasation occurred mainly towards the synovial fluid channel where the chemokine mix was added, while a similar and very low number of extravasated cells was found in both synovial compartments in control chips where chemokines were not added. We also demonstrated that endothelial preconditioning was crucial to promote monocyte extravasation in response to chemokines. This result is in line with data from other microfluidic extravasation models showing that shear stress levels similar to those applied here promote neutrophil extravasation and enhance CCL2 effect on monocyte extravasation [46, 47]. When interpreting these results, it should be underlined that the static condition was merely used as a negative control to investigate the combined effect of shear stress and TNF-α on monocyte extravasation, with these two elements considered as complementary factors applied to mimic, at least partially,

the *in vivo* situation that synovial endothelial cells encounter *in vivo*. On the other hand, the static condition cannot be considered as representative of any biomimetic situation since *in vivo* endothelial cells are always exposed to some level of shear stress.

As evidenced in the movies (supplementary materials S4 and S5), monocytes mostly extravasated in the first hours, suggesting that shear stress and TNF-α may induce a transient activation of endothelial cells, accordingly with data showing that VCAM-1 and ICAM-1 expression returns to basal levels soon after removing the stimulus [42]. The increase in cell permeability was another transient effect of the endothelial preconditioning and might contribute to explain this observation. Together with permeability experiments performed after the preconditioning phase, experiments conducted to verify whether the chemokine gradient could be maintained over the entire experimental time course (i.e. 18 h) showed a transient difference, which was lost after 60 min, between chips with preconditioned endothelium compared to chips in static conditions (supplementary material S6). The increase in endothelium permeability observed after the preconditioning phase most likely results from the reorganization of cell junctions and alterations in cell contractility which take place in the initial phases of monocyte extravasation under inflammatory conditions [35], as the ones that we aimed to model here using TNF-α. These events together with the steps that actively involve monocytes and their receptor-mediated interaction with endothelial cells, such as rolling and adhesion, as well as the signals generated by adherent monocytes further contributing to the dissociation of endothelial cell junctions is part of the extremely complex process that allows circulating monocytes to cross the endothelial barrier [12, 35].

To verify our hypothesis that inflammation-associated molecules released in synovial fluid can induce monocyte extravasation to the synovium, we determined extravasation in response to a pool of OA synovial fluids. OA synovial fluid showed a strong chemoattractant effect on monocytes, which most likely depends on the presence of pro-inflammatory cytokines and chemokines [45, 48], as differences in monocyte extravasation were observed comparing control and synovial fluid samples, independently from endothelial preconditioning or from the presence of tissue-specific cells. Despite the chemoattractant effect of OA synovial fluid on monocyte migration has been reported previously [49], our results provide the first direct evidence that OA synovial fluid is able to induce monocyte extravasation, which implies not only monocyte migration, but also crossing the endothelial barrier and invading the extravascular matrix. Unexpectedly, the number of extravasated monocytes was higher in samples without tissue-specific cells. We hypothesized that SFbs and ACs may

have reduced the local concentration of chemokines by receptor-binding and decreased the local oxygen and nutrient concentration contributing to this result. Albeit it is hard to identify a unique explanation for this difference, this result indicates that tissue-specific cells influence monocyte extravasation, supporting the effort to achieve a complex coculture.

Finally, the model was used to screen the ability of two chemokine receptor antagonists to inhibit monocyte extravasation. The first compound, RS-504393, is a potent antagonist for CCR2 that has been shown to ameliorate pathological changes in articular cartilage and bone when administered in mouse DMM models [50, 51]. The second compound, CVC, is a double antagonist which blocks both CCR2 and CCR5 and has provided interesting results when used in mouse models of liver and kidney diseases associated with an abnormal macrophage infiltration [52]. These antagonists were selected to demonstrate that the model could be exploited to investigate drug efficacy in inhibiting monocyte extravasation in an organotypic setting, bypassing the *in vivo* complexity. Our experiments demonstrated that both compounds reduce the number of extravasated monocytes in response to synovial fluid, with a stronger effect observed when both CCR2 and CCR5 were antagonized. It remains to be clarified if this ability implies a therapeutic efficacy of these antagonists in the context of OA, being monocyte infiltration to the synovium only one of the events that contribute to joint degeneration.

One of the limitations of this model is the lack of a compartment mimicking bone, a key element of the joint. When this study was designed, we considered including a bone compartment, based on our previously developed miniaturized 3D bone model [21]. However, adding osteoblasts and osteoclasts to the coculture would have posed significant complications to find common culture conditions suitable to all cell types. Hence, we focused mainly on synovium where monocyte extravasation takes place and cartilage that is the direct target of degenerative events triggered by infiltrating macrophages. Another limitation is that we have not clarified yet whether the extravasated monocytes exert a negative effect on the cartilage compartment. Studying the phenotype of extravasated monocytes in response to OA synovial fluid and their effect on the synovial and chondral compartment represents indeed one of our next plans.

5. Conclusions

In this study, we have developed and validated the first joint-on-a-chip model including vascularized synovium and articular cartilage, specifically designed to investigate the process of monocyte extravasation to synovium. Considering the future perspectives, this model can be used to dissect the biological mechanisms responsible for the abnormal macrophage

infiltration in synovium and find application to not only in the study of OA, but also of rheumatoid arthritis, where leukocyte infiltration represents a major disease hallmark. Additionally, the simultaneous presence of synovium and cartilage cells will allow investigating the crosstalk between extravasated monocytes/macrophages and tissue-specific cells in a microenvironment characterized by pathological synovial fluid.

Ethical statement

The study was approved by the Institutional Review Board (Ethical Committee of the IRCCS Ospedale San Raffaele; NCT03347500). Patient-derived materials including synovium, articular cartilage, blood, and synovial fluid were obtained from OA patients undergoing knee replacement, after the signature of informed consent.

Data availability statement

The data that support the findings of this study are openly available at the following URL/DOI: https://osf.io/68bwc/. Data will be available from 30 June 2021.

Acknowledgments

Conflict of interest

Authors have no competing interests to declare.

ORCID iDs

Carlotta Mondadori ⬤ https://orcid.org/0000-0003-3154-3414
Silvia Palombella ⬤ https://orcid.org/0000-0002-7628-5677
Shima Salehi ⬤ https://orcid.org/0000-0001-5655-5302
Giuseppe Talò ⬤ https://orcid.org/0000-0003-1976-5073
Roberta Visone ⬤ https://orcid.org/0000-0001-9077-1922
Marco Rasponi ⬤ https://orcid.org/0000-0003-3863-0596
Alberto Redaelli ⬤ https://orcid.org/0000-0002-9020-2188
Valerio Sansone ⬤ https://orcid.org/0000-0003-3206-4765
Matteo Moretti ⬤ https://orcid.org/0000-0002-7301-1208
Silvia Lopa ⬤ https://orcid.org/0000-0003-0410-5814

References

[1] Rahmati M, Mobasheri A and Mozafari M 2016 Inflammatory mediators in osteoarthritis: a critical review of the state-of-the-art, current prospects, and future challenges *Bone* **85** 81–90

[2] Buckwalter J A and Martin J A 2006 Osteoarthritis *Adv. Drug Deliv. Rev.* **58** 150–67

[3] Aspden R M and Saunders F R 2019 Osteoarthritis as an organ disease: from the cradle to the grave *Eur. Cell. Mater.* **37** 74–87

[4] Chen D, Shen J, Zhao W, Wang T, Han L, Hamilton J L and Im H J 2017 Osteoarthritis: toward a comprehensive understanding of pathological mechanism *Bone Res.* **5** 16044

[5] Scanzello C R and Goldring S R 2012 The role of synovitis in osteoarthritis pathogenesis *Bone* **51** 249–57

[6] Mathiessen A and Conaghan P G 2017 Synovitis in osteoarthritis: current understanding with therapeutic implications *Arthritis Res. Ther.* **19** 18

[7] Sokolove J and Lepus C M 2013 Role of inflammation in the pathogenesis of osteoarthritis: latest findings and interpretations *Ther. Adv. Musculoskelet. Dis.* **5** 77–94

[8] Malemud C J 2015 Biologic basis of osteoarthritis: state of the evidence *Curr. Opin. Rheumatol.* **27** 289–94

[9] Bondeson J, Blom A B, Wainwright S, Hughes C, Caterson B and van den Berg W B 2010 The role of synovial macrophages and macrophage-produced mediators in driving inflammatory and destructive responses in osteoarthritis *Arthritis Rheum.* **62** 647–57

[10] Berenbaum F 2013 Osteoarthritis as an inflammatory disease (osteoarthritis is not osteoarthrosis!) *Osteoarthr. Cartil.* **21** 16–21

[11] Elemam N M, Hannawi S and Maghazachi A A 2020 Role of chemokines and chemokine receptors in rheumatoid arthritis *ImmunoTargets Ther.* **9** 43–56

[12] Gerhardt T and Ley K 2015 Monocyte trafficking across the vessel wall *Cardiovasc. Res.* **107** 321–30

[13] Mondadori C, Crippa M, Moretti M, Candrian C, Lopa S and Arrigoni C 2020 Advanced microfluidic models of cancer and immune cell extravasation: a systematic review of the literature *Front. Bioeng. Biotechnol.* **8** 907

[14] Coughlin M F and Kamm R D 2020 The use of microfluidic platforms to probe the mechanism of cancer cell extravasation *Adv. Healthcare Mater.* **9** e1901410

[15] Boussommier-Calleja A, Atiyas Y, Haase K, Headley M, Lewis C and Kamm R D 2019 The effects of monocytes on tumor cell extravasation in a 3D vascularized microfluidic model *Biomaterials* **198** 180–93

[16] Kim H, Chung H, Kim J, Choi D-H, Shin Y, Kang Y G, Kim B-M, Seo S-U, Chung S and Seok S H 2019 Macrophages-triggered sequential remodeling of endothelium-interstitial matrix to form pre-metastatic niche in microfluidic tumor microenvironment *Adv. Sci.* **6** 1900195

[17] Lopa S, Colombini A, Sansone V, Preis F W and Moretti M 2013 Influence on chondrogenesis of human osteoarthritic chondrocytes in co-culture with donor-matched mesenchymal stem cells from infrapatellar fat pad and subcutaneous adipose tissue *Int. J. Immunopathol. Pharmacol.* **26** 23–31

[18] Lopa S, Leijs M J, Moretti M, Lubberts E, van Osch G J and Bastiaansen-Jenniskens Y M 2015 Arthritic and non-arthritic synovial fluids modulate IL10 and IL1RA gene expression in differentially activated primary human monocytes *Osteoarthr. Cartil.* **23** 1853–7

[19] Ragni E, Palombella S, Lopa S, Talo G, Perucca Orfei C, de Luca P, Moretti M and de Girolamo L 2020 Innovative visualization and quantification of extracellular vesicles interaction with and incorporation in target cells in 3D microenvironments *Cells* **9** 5

[20] Bersini S, Jeon J S, Dubini G, Arrigoni C, Chung S, Charest J L, Moretti M and Kamm R D 2014 A microfluidic 3D *in vitro* model for specificity of breast cancer metastasis to bone *Biomaterials* **35** 2454–61

[21] Bongio M, Lopa S, Gilardi M, Bersini S and Moretti M 2016 A 3D vascularized bone remodeling model combining osteoblasts and osteoclasts in a CaP nanoparticle-enriched matrix *Nanomedicine* **11** 1073–91

[22] Pauty J, Usuba R, Takahashi H, Suehiro J, Fujisawa K, Yano K, Nishizawa T and Matsunaga Y T 2017 A vascular permeability assay using an *in vitro* human microvessel model mimicking the inflammatory condition *Nanotheranostics* **1** 103–13

[23] Schwarz J, Bierbaum V, Merrin J, Frank T, Hauschild R, Bollenbach T, Tay S, Sixt M and Mehling M 2016 A microfluidic device for measuring cell migration towards substrate-bound and soluble chemokine gradients *Sci. Rep.* **6** 36440

[24] Raimondi M T, Boschetti F, Falcone L, Fiore G B, Remuzzi A, Marinoni E, Marazzi M and Pietrabissa R 2002 Mechanobiology of engineered cartilage cultured under a quantified fluid-dynamic environment *Biomech. Model. Mechanobiol.* **1** 69–82

[25] Arrigoni C, Lopa S, Candrian C and Moretti M 2020 Organs-on-a-chip as model systems for multifactorial musculoskeletal diseases *Curr. Opin. Biotechnol.* **63** 79–88

[26] Bersini S, Arrigoni C, Lopa S, Bongio M, Martin I and Moretti M 2016 Engineered miniaturized models of musculoskeletal diseases *Drug Discov. Today* **21** 1429–36

[27] Ahmed T A E, Dare E V and Hincke M 2008 Fibrin: a versatile scaffold for tissue engineering applications *Tissue Eng.* B **14** 199–215

[28] Akther F, Little P, Li Z, Nguyen N-T and Ta H T 2020 Hydrogels as artificial matrices for cell seeding in microfluidic devices *RSC Adv.* **10** 43682–703

[29] Morin K T and Tranquillo R T 2013 *In vitro* models of angiogenesis and vasculogenesis in fibrin gel *Exp. Cell Res.* **319** 2409–17

[30] Lai V K, Frey C R, Kerandi A M, Lake S P, Tranquillo R T and Barocas V H 2012 Microstructural and mechanical differences between digested collagen–fibrin co-gels and pure collagen and fibrin gels *Acta Biomater.* **8** 4031–42

[31] Lin S and Gu L 2015 Influence of crosslink density and stiffness on mechanical properties of type I collagen gel *Materials* **8** 551–60

[32] Coradin T, Wang K, Law T and Trichet L 2020 Type I collagen-fibrin mixed hydrogels: preparation, properties and biomedical applications *Gels* **6** 4

[33] Scotti C, Mangiavini L, Boschetti F, Vitari F, Domeneghini C, Fraschini G and Peretti G M 2010 Effect of *in vitro* culture on a chondrocyte-fibrin glue hydrogel for cartilage repair *Knee Surg. Sports Traumatol. Arthrosc.* **18** 1400–6

[34] Bachmann B, Spitz S, Schadl B, Teuschl A H, Redl H, Nurnberger S and Ertl P 2020 Stiffness matters: fine-tuned hydrogel elasticity alters chondrogenic redifferentiation *Front. Bioeng. Biotechnol.* **8** 373

[35] Wettschureck N, Strilic B and Offermanns S 2019 Passing the vascular barrier: endothelial signaling processes controlling extravasation *Physiol. Rev.* **99** 1467–525

[36] Vestweber D 2012 Relevance of endothelial junctions in leukocyte extravasation and vascular permeability *Ann. New York Acad. Sci.* **1257** 184–92

[37] Schnoor M, Alcaide P, Voisin M-B and van Buul J D 2015 Crossing the vascular wall: common and unique mechanisms exploited by different leukocyte subsets during extravasation *Mediators Inflamm.* **2015** 946509

[38] Wang X, Sun Q and Pei J 2018 Microfluidic-based 3D engineered microvascular networks and their applications in vascularized microtumor models *Micromachines* **9** 10

[39] McDonald K K, Cooper S, Danielzak L, Leask R L and Sperandio M 2016 Glycocalyx degradation induces a proinflammatory phenotype and increased leukocyte adhesion in cultured endothelial cells under flow *PLoS One* **11** e0167576

[40] Burns M P and de Paola N 2005 Flow-conditioned HUVECs support clustered leukocyte adhesion by coexpressing ICAM-1 and E-selectin *Am. J. Physiol. Heart Circ. Physiol.* **288** H194–204

[41] Uzarski J S, Scott E W, McFetridge P S and Mohanraj R 2013 Adaptation of endothelial cells to physiologically-modeled, variable shear stress *PLoS One* **8** e57004

[42] Chiu J-J, Lee P-L, Chen C-N, Lee C-I, Chang S-F, Chen L-J, Lien S-C, Ko Y-C, Usami S and Chien S 2004 Shear stress increases ICAM-1 and decreases VCAM-1 and E-selectin expressions induced by tumor necrosis factor-α in endothelial cells *Arterioscler. Thromb. Vasc. Biol.* **24** 73–9

[43] Tessier P, Audette M, Cattaruzzi P and McColl S R 1993 Up-regulation by tumor necrosis factor alpha of intercellular adhesion molecule 1 expression and function in synovial fibroblasts and its inhibition by glucocorticoids *Arthritis Rheum.* **36** 1528–39

[44] Krinninger P, Ensenauer R, Ehlers K, Rauh K, Stoll J, Krauss-Etschmann S, Hauner H and Laumen H 2014 Peripheral monocytes of obese women display increased chemokine receptor expression and migration capacity *J. Clin. Endocrinol. Metab.* **99** 2500–9

[45] Scanzello C R 2017 Chemokines and inflammation in osteoarthritis: insights from patients and animal models *J. Orthop. Res.* **35** 735–9

[46] Sharifi F *et al* 2019 A foreign body response-on-a-chip platform *Adv. Healthcare Mater.* **8** e1801425

[47] Lamberti G, Prabhakarpandian B, Garson C, Smith A, Pant K, Wang B and Kiani M F 2014 Bioinspired microfluidic assay for *in vitro* modeling of leukocyte–endothelium interactions *Anal. Chem.* **86** 8344–51

[48] Tsuchida A I, Beekhuizen M, T Hart M C, Radstake T R D J, Dhert W J A, Saris D B F, van Osch G J and Creemers L B 2014 Cytokine profiles in the joint depend on pathology, but are different between synovial fluid, cartilage tissue and cultured chondrocytes *Arthritis Res. Ther.* **16** 441

[49] Liu S C, Hsu C J, Fong Y C, Chuang S M and Tang C H 2013 CTGF induces monocyte chemoattractant protein-1 expression to enhance monocyte migration in human synovial fibroblasts *Biochim. Biophys. Acta* **1833** 1114–24

[50] Longobardi L *et al* 2017 Role of the C-C chemokine receptor-2 in a murine model of injury-induced osteoarthritis *Osteoarthr. Cartil.* **25** 914–25

[51] Raghu H *et al* 2017 CCL2/CCR2, but not CCL5/CCR5, mediates monocyte recruitment, inflammation and cartilage destruction in osteoarthritis *Ann. Rheum. Dis.* **76** 914–22

[52] Lefebvre E *et al* 2016 Antifibrotic effects of the dual CCR2/CCR5 antagonist cenicriviroc in animal models of liver and kidney fibrosis *PLoS One* **11** e0158156